Mon. Not. R. Astron. Soc. **301**, 81–94 (1998)

Cold dark matter variant cosmological models – I. Simulations and preliminary comparisons

Michael A. K. Gross,[1,2⋆] Rachel S. Somerville,[1,3⋆] Joel R. Primack,[1⋆] Jon Holtzman[4⋆] and Anatoly Klypin[4⋆]

[1]*Physics Department, University of California, Santa Cruz, CA 95064 USA*
[2]*Earth & Space Data Computing Division, Code 931, NASA/Goddard Space Flight Center, Greenbelt, MD 20771 USA*
[3]*Racah Institute of Physics, The Hebrew University, Jerusalem 91904, Israel*
[4]*Department of Astronomy, New Mexico State University, Las Cruces, NM 88001 USA*

Accepted 1998 July 16. Received 1998 July 3; in original form 1998 January 12

ABSTRACT

We present two matched sets of five dissipationless simulations each, including four presently favoured minimal modifications to the standard cold dark matter (CDM) scenario. One simulation suite, with a linear box size of $75\,h^{-1}$ Mpc, is designed for high resolution and good statistics on the group/poor cluster scale, and the other, with a box size of $300\,h^{-1}$ Mpc, is designed for good rich cluster statistics. All runs had 57 million cold particles, and models with massive neutrinos (CHDM-2ν) had an additional 113 million hot particles. We consider separately models with massive neutrinos, tilt, curvature, and a non-zero cosmological constant ($\Lambda \equiv 3H_0^2\Omega_\Lambda$) in addition to the standard CDM model. We find that the dark matter in each of our tilted $\Omega_0 + \Omega_\Lambda = 1$ (TΛCDM) model with $\Omega_0 = 0.4$, our tilted $\Omega_0 = 1$ model (TCDM), and our open $\Lambda = 0$ (OCDM) model with $\Omega_0 = 0.5$ has too much small-scale power by a factor of $\sim$2, while CHDM-2ν and SCDM are acceptable fits. In addition, we take advantage of the large dynamic range in detectable halo masses afforded by the combination of the two sets of simulations to test the Press–Schechter approximation. We find good fits at cluster masses for $\delta_{c,g} = 1.27$–1.35 for a Gaussian filter and $\delta_{c,t} = 1.57-1.73$ for a top hat filter. However, when we adjust δ_c to obtain a good fit at cluster mass scales, we find that the Press–Schechter model overpredicts the number density of haloes compared to the simulations by a weakly cosmology-dependent factor of 1.5–2 at galaxy and group masses. It is impossible to obtain a good fit over the entire range of masses simulated by adjusting δ_c within reasonable bounds.

Key words: cosmic microwave background – cosmology: theory – dark matter – large-scale structure of Universe.

1 INTRODUCTION

The *COBE* DMR detection of anisotropies in the cosmic microwave background (CMB) (Smoot et al. 1992) made it very clear that the 'standard' structure formation scenario of cold dark matter (Blumenthal et al. 1984; Davis et al. 1985) cannot simultaneously account for fluctuations on very large and very small scales. That model made several very restrictive assumptions about cosmological parameters – that space–time is homogenous, isotropic and globally flat; that there is no cosmological constant; that fluctuations from homogeneity are Gaussian-distributed and nearly scale-independent at horizon crossing; that the Hubble parameter $h \equiv H_0/(100\,\mathrm{km\,s^{-1}\,Mpc^{-1}})$ is 0.5; and that the number of free parameters is minimized. The obvious fixes to the problem of excess small-scale power (when normalizing power spectra to the *COBE* anisotropy) are to make one of the following modifications to the model:

(i) tilt the primordial spectrum,
(ii) allow a non-zero cosmological constant but retain globally flat geometry,
(iii) allow the universe to be open,
(iv) add hot dark matter (i.e. neutrinos with masses of a few eV), or
(v) lower the Hubble parameter much further ($h \sim 0.3$–0.4).

Each of these modifications adds only one free parameter to the cosmology. In this paper, we consider the most viable models from each class above except the last, and simulate them with an N-body code in two suites, with equivalent initial conditions across all the

⋆E-mail: gross@fozzie.gsfc.nasa.gov (MAKG); rachels@alf.fiz.huji.ac.il (RSS); joel@ucolick.org (JRP); holtz@nmsu.edu (JH); aklypin@nmsu.edu (AK)

models. We do not consider a 'low-H_0' model (Bartlett et al. 1995) because of increasingly solid observational evidence that $h \gtrsim 0.5$.

Deciding on cosmological parameters is to some extent an iterative process. Much can be done using the Press–Schechter (1974) approximation, but the assumptions that go into it are not necessarily realistic (for example, spherical symmetry – see Jain & Bertschinger 1994 and Monaco 1995). Therefore, it is useful as a *first approximation* to calculating the mass functions, and we use it to perform an approximate cluster normalization, using guesses about other cosmological parameters. We run a set of simulations and use them to test the Press–Schechter approximation, and make several preliminary comparisons to observational data. In a companion paper (Gross et al., in preparation), we recalibrate the Press–Schechter approximation and use it to derive refined estimates of model normalization and Ω_0 from several different data sets, and make more careful comparisons to cluster abundance. Subsequent papers will use simulations based on the refined normalizations.

In Section 2.1, we describe our specific models from each class of CDM-variant models and explain why we chose the parameters as we did. In Section 2.2, we briefly describe the implementation of the particle–mesh algorithm we used for this study. We explain our halo-finding algorithm and the effect of mass resolution upon it in Section 3 and report the simulation results in Section 4. Finally, in Section 5, we present our conclusions.

2 SIMULATIONS

2.1 Models

Given the long list of modifications to the cold dark matter (CDM) scenario in the previous section, we could construct a model by adjusting *every* parameter in order to fit all the available observational data. However, in addition to being aesthetically displeasing, the physical significance of such a model would be unclear. As a result, we have tried to minimize the number of modifications to the relatively simple standard cold dark matter (SCDM) scenario by investigating each of the modifications mentioned above in a separate model. The exceptions to this policy are that, in addition to any one of modifications (ii)–(iv), we allow a small tilt, up to $n = 0.9$, in order to simultaneously fit the *COBE* and cluster data, and we allow the Hubble parameter to be adjusted within reasonable observational bounds according to the requirements of the model. Larger tilts are not allowed because they tend to cause disagreements with high-multipole cosmic microwave background data.

We explore the large parameter space by running a large suite of linear calculations and comparing the output to appropriate observational constraints. Constraints that we consider in choosing model parameters for more detailed non-linear analysis are as follows.

(i) The abundance of Abell clusters, as measured by X-ray temperature profiles (White, Efstathiou & Frenk 1993; Biviano et al. 1993, hereafter WEF93 and BGGMM93, respectively). We assume that cluster masses may be underestimated by up to a factor of two, motivated by results from cluster density mapping with gravitational lensing (Squires et al. 1996, 1997; Miralda-Escudé & Babul 1995; Wu & Fang 1996; Wu & Fang 1997, Fig. 1).

(ii) Microwave background anisotropies for $\ell \lesssim 800$ (Fig. 2) as measured by several recent CMB detection experiments (Tegmark 1996; Netterfield et al. 1997; Scott et al. 1996; Platt et al. 1997; Fig. 2).

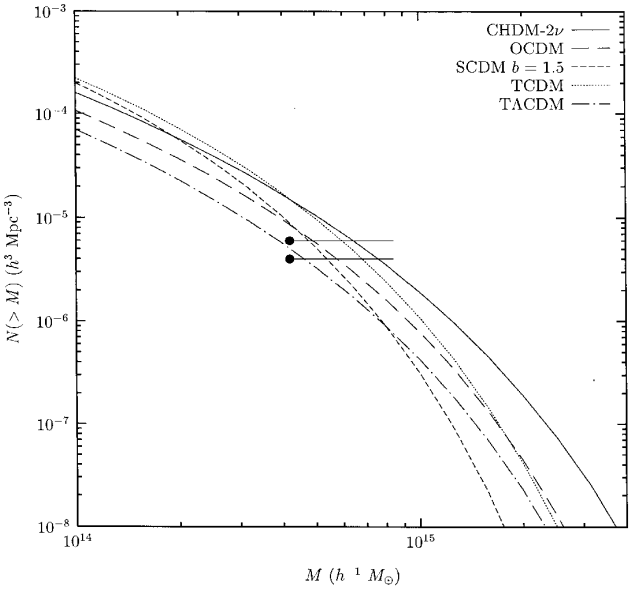

Figure 1. Expected mass functions for all models estimated from the Press–Schechter approximation with a Gaussian filter, using $\delta_{c,g} = 1.5$ for the model with massive neutrinos and $\delta_{c,g} = 1.3$ for all other models. The two data points shown correspond to observational estimates of cluster abundance (WEF93, BGGMM93). Note that cluster density mapping via gravitational lensing (Squires et al. 1996; Squires et al. 1997; Miralda-Escudé & Babul 1995; Wu & Fang 1997) may indicate that X-ray masses are systematically low, and the masses can plausibly be raised by a factor of up to two, which corresponds to the horizontal line on the right of each cluster data point.

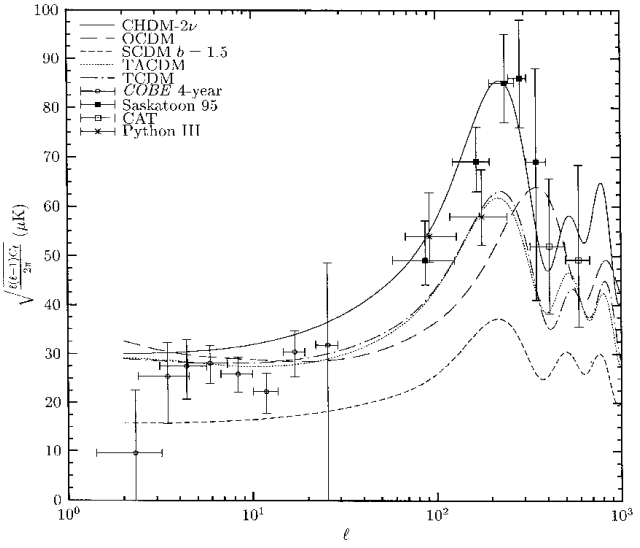

Figure 2. Model comparison to cosmic microwave background. All models except SCDM are consistent with *COBE* four year data (Górski et al. 1996; Górski, private communication). Circles, solid squares, open squares and asterisks are the *COBE* four-year power spectrum (Tegmark 1996), Saskatoon 1995 results (Netterfield et al. 1997), CAT detection (Scott et al. 1996) and Python III results (Platt et al. 1997), respectively. Not shown are systematic normalization errors of 14 and 20 per cent, for Saskatoon and Python III, respectively. The curves are all calculated using the CMBFAST program of Seljak & Zaldarriaga (1996). Cosmological parameters correspond to models considered in this paper, except for SCDM. The normalization is adjusted so that the low harmonics match the output of our linear code. CMBFAST is capable of calculating larger multipoles than our linear code. SCDM is shown here with $\Omega_b = 0.1$, since all the high-ℓ features in the CMB spectrum are dependent upon baryon interactions, but was actually simulated with no baryons.

Table 1. Model parameters and linear results for both simulation suites.

Model	Age[a]	h[b]	Ω_0	Ω_c	Ω_b	Ω_ν	Ω_Λ	n[c]	N_ν[d]	σ_8[e]	$\tilde{\sigma}_8$[f]	V_{50}[g]	N_{cl}[h]
observations												375	5×10^{-6}
1-σ errors												85	2×10^{-6}
CHDM-2ν	13.0	0.5	1.0	0.7	0.1	0.2	0.0	1.0	2	0.719	0.719	399	6×10^{-6}
OCDM	12.3	0.6	0.5	0.431	0.069	0.	0.0	1.0	0	0.773	0.581	254	3×10^{-6}
SCDM	13.0	0.5	1.0	1.0	0.0	0.0	0.0	1.0	0	0.667	0.667	192	2×10^{-6}
TCDM	14.5	0.45	1.0	0.9	0.1	0.0	0.0	0.9	0	0.732	0.732	270	5×10^{-6}
TΛCDM	14.5	0.6	0.4	0.365	0.035	0.0	0.6	0.9	0	0.878	0.572	335	2×10^{-6}

[a] Time since the big Bang in Gyr.
[b] Presumed Hubble parameter, in units of $100\,\mathrm{km\,s^{-1}\,Mpc^{-1}}$.
[c] 'Tilt' of the primordial spectrum; $P(k)\propto k^n$.
[d] Number of massive neutrinos presumed. The equivalent mass of a neutrino is $m_\nu = \frac{\Omega_\nu h^2}{N_\nu}\times 92\,\mathrm{eV}$.
[e] rms mass fluctuation in a sphere of radius $8\,h^{-1}$ Mpc.
[f] $\tilde{\sigma}_8 \equiv \sigma_8\Omega_0^{0.46-0.10\Omega_0}$ for $\Lambda = 0$ models, and $\sigma_8\Omega_0^{0.52-0.13\Omega_0}$ for $\Omega_\Lambda + \Omega_0 = 1$ models. Eke et al. (1996) calculate $\tilde{\sigma}_8 = 0.52 \pm 0.04$ in order to fit cluster temperatures assuming $\beta \equiv \langle KE\rangle_{dm}/\langle KE\rangle_{gas} = 1$. However, new simulations (Frenk et al. 1998) show that $\beta \approx 1.17$, corresponding to $\tilde{\sigma}_8 = 0.61 \pm 0.05$.
[g] rms velocity in a sphere of radius $50\,h^{-1}$ Mpc (Dekel et al. 1997). Note that the observational value is for one particular $50\,h^{-1}$ Mpc sphere around the Local Group, and the simulation values are the rms value for a distribution of randomly placed spheres. These are not the same, so we cannot use the observations to rigorously define confidence limits for the simulation quantities.
[h] Estimated number density of clusters of mass $> 6\times10^{14}\,h^{-1}\,M_\odot$, in $h^3\,\mathrm{Mpc^{-3}}$, from Press–Schechter theory with a Gaussian window function. $\delta_{c,g}$ is 1.5 for CHDM models (Walter & Klypin 1996; Borgani et al. 1997b) and 1.3 for all other models (Liddle et al. 1996, KPH96). Masses near the centre of the allowable range for cluster data (WEF93, BGGMM93) are used. Note that uncertainties in the masses of measured clusters mean that the masses for which densities were measured could shift coherently up to a factor of two above the reported value of $4.2\times10^{14}\,h^{-1}\,M_\odot$. This is a naive approach which we use only for our first iteration of model parameters. We use more sophisticated methods in Gross et al. (in preparation).

(iii) 'Bulk flow' peculiar velocity measurements and resulting constraints on the power spectrum (Dekel et al., in preparation; Kolatt & Dekel 1997; Fig. 3). The linear estimates of these parameters are shown in Table 1 and in Figs 1–4 for the models we consider.

In most of the previous work with modified CDM models, the most 'extreme' values of the model parameters have been chosen (i.e. as far from SCDM as was considered observationally plausible). For example, low-Ω_0 models typically have values of $\Omega_0 \sim 0.2-0.3$. However, in every case, while solving some of the problems with SCDM, this introduces new problems or conflicts with other observational constraints. Thus our approach will be somewhat different. We use our previous experience with linear and non-linear tests of CDM-variant models, as well as the published results of others, to find models that represent a 'middle ground' between SCDM and the most extreme version of the particular class of model. In this way, we hope to choose the 'best' rather than the most extreme case, and to identify models that agree with the widest possible range of observations.

For most models, we presume a baryon abundance of $\Omega_b = 0.025h^{-2}$, consistent with the Tytler, Fan & Burles (1996) cosmic deuterium abundance measurement.[1] Normalization is accomplished by calculating low multipoles using an enhanced version of the linear code from Holtzman (1989) and comparing to the four-year *COBE* DMR anisotropy measurements (Górski et al. 1996; Górski, private communication).

[1] Burles & Tytler (1997, 1998) have very recently remeasured the deuterium abundance and found it to be 20 per cent lower, 0.019 ± 0.001. This makes a very small change in the power spectrum, and the most significant effect is to make agreement with high-ℓ cosmic microwave background measurements (Fig. 2) more difficult. The height of the first Doppler peak depends strongly on Ω_b.

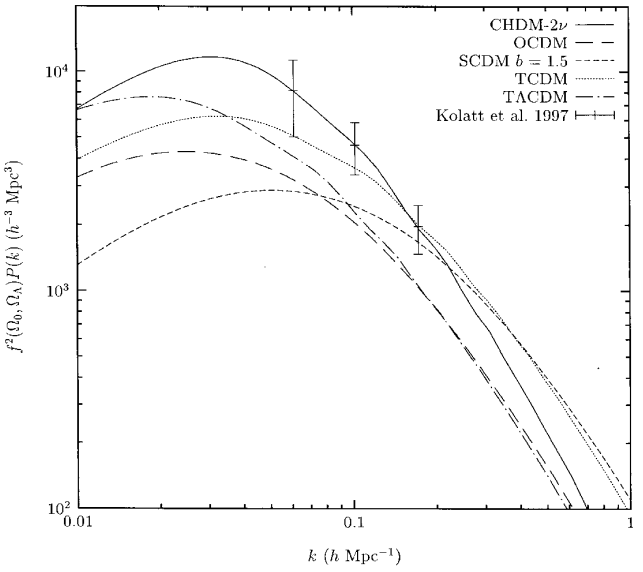

Figure 3. Linear power spectrum comparison to bulk-flow measurements. The curves are all a magnification of Fig. 4, multiplied by $f^2(\Omega_0,\Omega_\Lambda)\equiv(a\dot{D}/\dot{a}D)^2$. The three data points are from Kolatt & Dekel (1997). $f(\Omega_0,\Omega_\Lambda)$ was calculated exactly, using equation (C.3.14) of Gross (1997) and its analytic derivative.

For comparison to other studies, we also simulated the SCDM model with bias $b = \sigma_8^{-1} = 1.5$. That model is intended to approximately match observed cluster abundances at the cost of being inconsistent with the *COBE* anisotropy measurements. For this model, we presumed there were no baryons in the Universe, and used the BBKS transfer function (Bardeen et al. 1986) used in

previous studies, that is,

$$P(k) = Ak\frac{[\ln(1+2.34q)]^2}{(2.34q)^2}[1+3.89q+(16.1q)^2 + (5.46q)^3+(6.71q)^4]^{-1/2} \quad (1)$$

with $q = kh^{-2}$ and A adjusted so that the rms fractional variance in mass in spheres of radius $8\,h^{-1}$ Mpc estimated using linear theory is $\sigma_8 = 0.667$.

The simplest way to solve the problem of excess power on small scales is by 'tilting' the spectrum, that is, by changing the Ak factor in equation (1) to Ak^n, with $n < 1$. However, the price paid is that choosing $n < 1$ also reduces the amplitude of the first 'Doppler peak' in the small-angle cosmic microwave background spectrum. We find that $n \sim 0.9$ is the largest allowable tilt that is still marginally consistent with the large-multipole cosmic microwave background data. With $n = 0.9$, when we *COBE* normalize the model we find that it tends to overproduce clusters at $M = 6\times 10^{14}\,h^{-1}\,\mathrm{M}_\odot$ according to the Press–Schechter estimate, unless we use a rather low value of the Hubble parameter, $h = 0.45$. Although this is not favoured by most of the current observational data, we conclude that this choice of parameters constitutes the best compromise amongst the observational constraints that we have imposed.

Another fix is to add a little hot dark matter, usually assumed to be in the form of a massive neutrino. Previously studied versions of this class of model typically postulate a single species of neutrino with significant mass, and a fraction $\Omega_\nu = 0.3$ of the critical density in the form of hot dark matter (HDM). This model was ruled out, based on its inability to reproduce the observed abundances of damped Lyman α systems (DLAS) at $z \sim 3$ (Kauffmann & Charlot 1994; Klypin et al. 1995). Models with lower fractions of hot dark matter ($\Omega_\nu = 0.2$) are more plausibly consistent with constraints from DLAS (Klypin et al. 1995), but still have too much small-scale power and thus overproduce clusters at $z = 0$. However, as pointed out by Primack et al. (1995; see also Pogosyan & Starobinsky 1995), if the hot dark matter is divided into two species of neutrino with equal masses, the power on cluster scales is reduced by 20 per cent without affecting smaller or larger scales. This lowers cluster abundances without worsening potential early structure formation problems (small-scale power) or compromising the *COBE* normalization. We find reasonable agreement with observed cluster abundances with $\Omega_\nu = 0.2$, $N_\nu = 2$, $h = 0.50$, and $n = 1$; or alternatively, with a small tilt ($n = 0.9$) and a higher Hubble parameter ($h = 0.6$). We chose the former, based on concerns about the age of the Universe. However, we ran the simulations before the *Hipparcos* recalibration of the age of globular clusters (Reid 1997; Gratton et al. 1998; Chaboyer et al. 1998). This constraint has now been considerably weakened, and $h = 0.6$ or even 0.65 would lead to ages consistent with the present estimates.

The $\Omega_\Lambda \neq 0$ class of models has been well studied, typically with $\Omega_0 = 0.3$ and $h \sim 0.65$–0.7. However, analysis of earlier N-body simulations has shown that when non-linear effects are included, this model produces a power spectrum/correlation function with too high an amplitude on small spatial scales compared to observations, unless galaxies are strongly anti-biased with respect to the dark matter (Klypin, Primack & Holtzman 1996, hereafter KPH96; Jenkins et al. 1998). Ghigna et al. (1997) have also shown that the void probability function for this model is in disagreement with observations. Therefore we have chosen a model with a slightly higher value of the matter density ($\Omega_0 = 0.4$) and a tilt ($n = 0.9$) to reduce small-scale power and correlations (TΛCDM).

Many observers favour an open cosmology and a high Hubble parameter, consistent with local density estimates and the Hubble Key Project. The lowest reasonable value of Ω_0, given initial Gaussian fluctuations as assumed in all CDM-variant models considered here, is constrained to be above 0.3 at $\gtrsim 4\sigma$ confidence (Nusser & Dekel 1993; cf. also Dekel & Rees 1994; Bernardeau et al. 1995). We adopt $\Omega_0 = 0.5$ as a 'reasonable' value for open CDM (OCDM), noting that even this relatively high Ω_0 leads to a power spectrum lower than that indicated by the POTENT analysis (Kolatt & Dekel 1997; see also Fig. 3). Our linear code is not capable of determining low multipole cosmic microwave background fluctuations for OCDM, as it uses a plane wave expansion that is only appropriate for flat cosmologies. Instead, we use fitting functions for the normalization $\delta_H(\Omega_0)$ and the transfer function $T(k)$ given by Liddle et al. (1996, hereafter LLRV96).[2]

Fig. 1 summarizes the expected mass functions on the group and cluster mass scales, as estimated from the Press–Schechter approximation, with a Gaussian filter. Using the calibration with N-body simulations from Borgani et al. (1997b), we use $\delta_{\mathrm{c,g}} = 1.5$ for the model with massive neutrinos and $\delta_{\mathrm{c,g}} = 1.3$ for all other models, in this figure (but cf. Table 3, below, for best-fitting $\delta_{\mathrm{c,g}}$ and $\delta_{\mathrm{c,t}}$ to our simulation results). The observational cluster abundance estimates plotted are in reasonable agreement with these mass functions, especially if the mass estimates are low as indicated by some gravitational lensing estimates.

In Fig. 2, we compare each model to several recent CMB measurements, using the CMBFAST program of Seljak & Zaldarriaga (1996). We also show the four most recently announced CMB results on the figure. Not shown are systematic calibration errors of 14 per cent for Saskatoon and 20 per cent for Python III. Note that the OCDM model is strongly inconsistent with Saskatoon points, and our choice of $\Omega_0 = 0.5$ is at the 95 per cent confidence lower limit for an open model (Lineweaver & Barbosa 1998). Also note that the models with even the relatively mild tilt of $n = 0.9$ are at best in marginal agreement with the Saskatoon data around the first Doppler peak.

Fig. 4 shows the linear power spectra at the present epoch. As one might expect, all the spectra nearly cross at a wavenumber of a few tenths $h\,\mathrm{Mpc}^{-1}$, corresponding to cluster scales. Also, we show some of the window functions used in the normalization procedure described above.

In Fig. 3, we compare our models to the matter power spectrum recently measured from bulk flows by Kolatt & Dekel (1997). We only use the three data points that Kolatt & Dekel use for their own statistical analysis, because for larger wavenumbers smoothing lowers the power significantly. SCDM disagrees at about the 2.5σ level, also reflected in its low value of V_{50} in Table 1. OCDM and TΛCDM disagree because the value of $P(\sim 0.1\,h\,\mathrm{Mpc}^{-1})$ is fixed by comparing the observed density of clusters (WEF93, BGGMM93, Borgani et al. 1997a) to the Press–Schechter prediction, and they

[2] After we ran this model, LLRV96 was superseded by Bunn & White (1997) and Hu & White (1997). The σ_8 values in those papers agree to high precision with LLRV96 if one lowers Ω_b from 0.025 to $0.015\,h^{-2}$, which Bunn & White (1997) favour anyway. However, the transfer function shapes are somewhat different, and the LLRV96 normalization is to the *COBE* 2-yr data, so the power on scales of a few hundred h^{-1} kpc may be up to 20 per cent low compared to Bunn & White (1997) and Hu & White (1997). Using a BBKS-style fit as all three papers do, rather than integrating the Boltzmann equation directly, introduces an error of similar magnitude, even with the improved shape parameter described in Hu & Sugiyama (1996, equation D-29). We therefore neglect the difference between the Bunn & White (1997) and LLRV96 spectra.

have low values of $f(\Omega_0, \Omega_\Lambda) \equiv \dot{D}a/D\dot{a} \approx \Omega_0^{0.6}$, where $D(\Omega_0, \Lambda, t)$ is the linear growth factor and $a(t)$ is the expansion parameter. The combination of cluster abundances and bulk-flow power spectrum measurements favours $f \sim 1$, for the currently favoured classes of CDM variant models.

There is currently significantly controversy over the proper normalization of models, and our OCDM and TΛCDM normalizations are higher than the recent fits reported in Eke, Cole & Frenk (1996), based on cluster X-ray temperature distributions (Henry & Arnaud 1991),[3] though they are consistent with the older analyses of WEF93 and the new cluster velocity dispersion measurements of Borgani et al. (1997a). Pen (1998) has reanalysed the Eke et al. (1996) calculation, and he gets slightly higher low-Ω_0 normalizations of $\sigma_8 = 0.86$ and 0.72 for our TΛCDM and OCDM models, respectively. These normalizations are close to those we have chosen (Table 1).

2.2 Algorithm

A classic problem with gravitational simulations is the 'overmerging' problem, where small-scale structure in highly overdense regions is not resolved. Part of the problem is physical – real galaxies form much denser cores than dissipationless haloes can, because the baryons can dissipate energy (but cf. Klypin, Gottlöber & Kravtsov 1997a). Aside from that, numerical limitations can make the problem vastly worse. There are two numerical effects to consider: force resolution and sampling of initial conditions and bound structures. Improving either of these requires vast amounts of memory and processing time, so there is an inherent trade-off.

Recently, the more popular approach has been to improve the forces by using hybrid (Hockney & Eastwood 1988; Couchman 1991; Xu 1995, for example) or adaptive-mesh (Kravtsov, Klypin & Khokhlov 1997, for example) force solvers, at the expense of either poor sampling of initial fluctuations or small box sizes. We choose a complementary approach, in which we try to balance the sampling of density in a large box with force resolution. We still require a large dynamic range in order both to sample small scales well and simultaneously to simulate a large volume for comparison to redshift surveys. Since the two requirements imply an enormous number of particles, computer time limitations force us to use the *fastest* code available. We chose a standard particle-mesh (Hockney & Eastwood 1988) algorithm, parallelized to run on a distributed-memory message-passing system.[4] This type of code produces adequate forces at about 1.5 grid cells [Klypin, Nolthenius & Primack 1997b (hereafter KNP97), appendix A], but we double this distance to be conservative. So, we require that we have 3^3 times as many grid cells as particles, for the high-resolution suite. We choose a grid cell size of $65\,h^{-1}$ kpc, with $N_g = 1152^3$ grid cells and $N_p = 384^3 = 57$ million 'cold' particles. For the large-volume case, we wish to follow the dynamics only of clusters of galaxies, so we can afford to coarsen the density grid slightly. We find that a cell size of $390\,h^{-1}$ kpc is adequate for following the dynamics of $\gtrsim 10^{14}\,h^{-1}\,M_\odot$ objects, and expect information about smaller objects to come from the high-resolution simulations. The slight coarsening of the density resulted in a substantial advantage in running time.

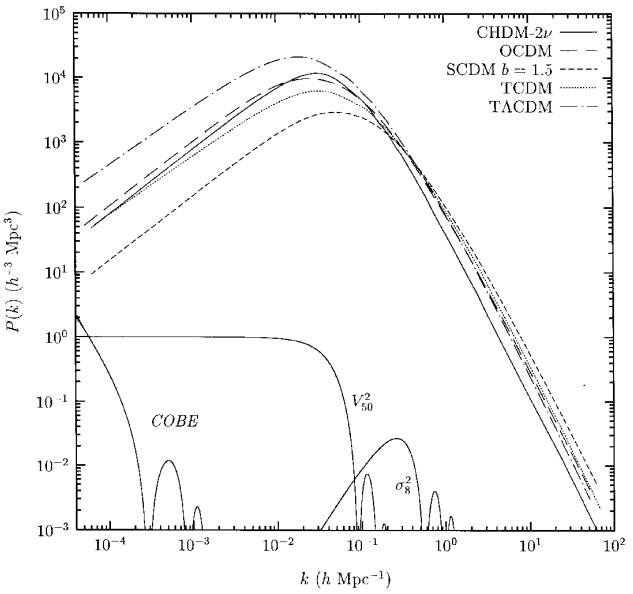

Figure 4. Linear power spectra used in our simulation suites. Also shown are two of the window functions used in normalizing the models: $k^2W^2(rk)$ with $r = 8\,h^{-1}$ Mpc for σ_8^2 and $W^2(rk)$ with $r = 50\,h^{-1}$ Mpc for V_{50}^2. Here $W(x) = 3[\sin(x) - x\cos(x)]x^{-3}$. Also shown (for illustrative purposes only) is the equivalent window function for approximate *COBE* normalization using the pure Sachs–Wolfe effect, $j_{10}^2(d_h k)/(2\pi d_h^2 k^2)$ where $j_{10}(x)$ is the 10th order spherical Bessel function and d_h is the horizon distance. The version plotted has the amplitude raised by a factor of 100 for visibility and uses $d_h = 2c/H_0 = 6000\,h^{-1}$ Mpc, which is appropriate for $\Omega_0 = 1$. For OCDM, the horizon distance is $7470\,h^{-1}$ Mpc and for TΛCDM, it is $8810\,h^{-1}$ Mpc, so the window function moves a small distance to smaller k in those cases. A similar window function for cluster abundance doesn't exist because it doesn't have the form of a convolution. In an extremely rough sense, the scales are comparable to those sampled by σ_8.

Initial conditions were calculated using a parallelized Zel'dovich (1970) approximation. For cold+hot dark matter (CHDM) models, we started with a uniform grid of cold particles, and two neutrinos at the position of every cold particle. Cold particles and neutrinos were offset from the grid using separate cold+baryon and hot power spectra, and consistent velocities were derived from the offsets using scale-dependent linear growth rates calculated by a refinement of the Holtzman (1989) code. In addition, equal and opposite random thermal velocities were chosen for each pair of neutrinos from a redshifted relativistic Fermi–Dirac distribution (Klypin et al. 1993).

We adopted the form of the equations of motion used in Kates, Kotok & Klypin (1991) generalized to arbitrary cosmology:

$$\nabla^2\phi = \frac{3}{2a}\delta \equiv \frac{3}{2a}\frac{\delta\rho}{\Omega\rho_c}, \tag{2}$$

$$\frac{d\boldsymbol{p}_i}{da} = -\dot{a}\nabla\phi(\boldsymbol{x}_i), \tag{3}$$

and

$$\frac{d\boldsymbol{x}_i}{da} = \frac{\boldsymbol{p}_i}{a^2\dot{a}}, \tag{4}$$

where $\dot{a}$ is given by the Friedmann equation with time variable $H_0 t$,

$$\dot{a} = a^{-1/2}\sqrt{\Omega_c + \Omega_\nu + \Omega_\Lambda a^3 + \Omega_k a}. \tag{5}$$

[3]Note that Eke et al. (1996) discovered two compensating errors in the Henry & Arnaud (1991) analysis: an arithmetical error of a factor of 4.2 and a binning error of a factor of about 4 in the other direction. The errors have also been noted in Viana & Liddle (1996).

[4]Specifically, the Cornell Theory Centre SP2, but the code is portable to any system supporting MPI, including heterogeneous workstation clusters and most modern supercomputers.

Table 2. Simulation parameters for both simulation suites.

Suite	Box size h^{-1} Mpc	$N_{\rm cells}$	Cell size h^{-1} kpc	$N^a_{\rm cold}$	$M^b_{\rm cold}$ $(\Omega_{\rm c}+\Omega_{\rm b})\,h^{-1}\,{\rm M}_\odot$	$N_{\rm steps}$	$M^c_{\rm min}$ $\Omega_0\,h^{-1}\,{\rm M}_\odot$	f^d
high res	75	1152^3	65	384^3	2.09×10^9	200	3.4×10^{11}	0.078
low res	300	768^3	390	384^3	1.34×10^{11}	150	7.3×10^{13}	0.043

[a]Number of cold particles; for models with massive neutrinos, $N_{\rm hot}=2N_{\rm cold}$.
[b]Mass of cold particles; for models with massive neutrinos, $M_{\rm hot}=M_{\rm cold}\Omega_\nu/2(\Omega_{\rm c}+\Omega_{\rm b})$.
[c]Halo detection cut-off, from the restriction that haloes must be larger than the grid size.
[d]Fractional error in mass for the smallest haloes identifiable.

Time discretization was a standard 'leapfrog' scheme (cf. Hockney & Eastwood 1988), with even steps in the expansion parameter a. To reduce the expense of the simulations, the time-step was chosen only to stabilize bound structures at the final time-step, rather then keep *all* structures on the scale of the grid spacing stable. This is only a problem for the cores of clusters, which have the highest velocities. For clusters, we presume an upper bound of particle velocities of $1200\,{\rm km\,s^{-1}}$ today and a minimum diameter of any given bound structure equal to the linear cell size. Stability for such an object requires that particles take at least one time-step to traverse the object. So, the required condition is

$$\Delta a \equiv \dot{a}\Delta t \lesssim \frac{H_0 L}{N_{\rm g}^{1/3} v_{\rm max}} \tag{6}$$

independent of cosmology because the condition is evaluated at the present epoch and H_0L is chosen to be the same for all models. Plugging in $v_{\rm max}=1200\,{\rm km\,s^{-1}}$, $H_0L=7500\,{\rm km\,s^{-1}}$ and $N_{\rm g}=1152^3$ gives $\Delta a\lesssim 0.005$, or 200 time-steps for the high-resolution suite. Such a low $v_{\rm max}$ will not model the interiors of clusters well, since they are observed to have velocity dispersions larger than that, but to remain bound to the cluster, particles have the much looser requirement that they not traverse the *whole cluster* in one time-step. As large cluster radii are up to about 50 grid cells, the effective stability limit is 20 per cent of the speed of light inside a large cluster, for the high-resolution suite, presuming that the cluster is adequately modelled by an isothermal sphere. We checked that the choice of time-step was adequate by running a $25\,h^{-1}$ Mpc box CHDM-2ν simulation with 384^3 grid cells (which has the same $65\,h^{-1}$ kpc cell size as the high-resolution suite) for 200 time-steps and for 300 time-steps. The resulting mass functions were not significantly different. For the large-volume suite, clusters do not cover nearly as many cells as in the high-resolution suite, and so the velocity limit is much higher. Our choice of 150 time-steps corresponds to a limiting speed of $5000\,{\rm km\,s^{-1}}$ if particles are not to cross one cell in a time-step. The suite parameters are summarized in Table 2.[5]

The Zel'dovich (1970) approximation is only valid when the rms fluctuations are much less than 1. In practice, one picks a starting time early enough so that linear theory brings the rms fluctuations well below 1. The initial time was chosen so that the rms overdensity on the grid scale was $\delta_{\rm rms}\lesssim 0.2$. This was $z=30-60$, depending on the model. Particle data and halo catalogues were stored at four equally spaced intervals in a during execution. The large-volume simulation suite used the same starting times as the high-resolution suite even though they could have been started somewhat later because of the poorer resolution. The extra computation involved is about one time-step and is therefore negligible.

Random numbers are necessary in order to model inflation-generated Gaussian fluctuations and random phases in the density field. Such randomness introduces highly significant variation from simulation to simulation, commonly referred to as 'cosmic variance'. Because we can only observe one universe, quantifying the effect of cosmic variance is very important and is a separate issue from variations between models due to different physics. In these suites, we have separated the effects by picking a single random number seed for each suite, checking that the largest 26 waves do not have any fluctuations larger than a factor of 2, and rerunning one model with a different seed. That is, within each suite, the random numbers for each model within a suite are all the same, and large wavelength fluctuations are restricted to a smaller range than Gaussian statistics would permit, in an attempt to prevent rare statistical flukes from compromising expensive simulations (as happened in Klypin et al. 1993). This means the structures are approximately in the same place, and when one also considers the cluster abundance criterion discussed in Section 2.1 there is roughly the same number, distribution and positions of $5\times10^{14}\,h^{-1}\,{\rm M}_\odot$ clusters in all the models in a given suite. Note that the models do have different power spectra and fluctuation growth rates, so distributions can differ for objects with different masses.

3 DARK MATTER HALOES

3.1 Halo-finding algorithm

We identify dark matter haloes using a spherical overdensity algorithm similar to that of KNP97, with some of the limitations removed.

(i) We define candidate haloes as the centres of all density maxima containing an overdensity greater than $\delta\equiv\delta\rho/\Omega_0\rho_{\rm c}=50$. A density maximum is defined as a cell the density of which is greater than its six Cartesian neighbours. Just in case there are other haloes hiding in those six neighbours, we also consider each of them to be candidates. Note that the finite grid size (as in all other grid-based halo finders, such as DENMAX, Gelb & Bertschinger 1994) will introduce a minimum separation between haloes, which may cause small haloes to be missed, which in turn will require a mass cut.

(ii) Each candidate halo then has the location of its centre set iteratively to the centre of mass of all the particles inside a sphere of diameter equal to the cell size ($65\,h^{-1}$ kpc in our high-resolution case). Haloes are expected to have a minimum size of the order of the grid size, so this procedure moves the candidate halo to the peak of the density maximum. Of course, since we have defined more

[5]Though the implementation, and especially parallelization, of the two-species particle mesh code described above is much less trivial than one might suppose, discussion of the code has been omitted for space considerations. The interested reader may find a detailed description of the code, its implementation on the Cornell SP2, and several code tests in Gross (1997).

than one candidate for each detected maximum, some candidates will converge on the same halo. The smaller mass object in a given pair is removed if the distance between the centres of mass is less than half the grid spacing.

(iii) We perform a central overdensity cut. All haloes that do not enclose a mean overdensity sufficient for virialization according to the spherical collapse model (see Gross 1997, appendix C, and references therein) at the end of the centre-of-mass detection phase are presumed not to be virialized objects and are discarded. Typically, this reduces the number of haloes by a factor of 2–3, though the number is model dependent.

(iv) We now estimate the radius at which the mean enclosed overdensity $\delta \equiv \delta\rho/\Omega\rho_c$ falls to δ_{vir}, the virial radius of the halo in spherical infall models.[6] For each halo, we count the number of particles within five radii up to five grid cells ($325\,h^{-1}$ kpc in this case) away from the centre, convert that to density, and interpolate the radius at which $\delta = \delta_{vir}(r_{vir})$ using power-law cubic splines. If five radii is not large enough to enclose r_{vir}, we search five more radii, each twice as long as the original radii. This is repeated until we enclose r_{vir}.

(v) We define the mass of the halo as the mass enclosed in r_{vir}. The velocity is the mean velocity of all the particles within r_{vir}.

(vi) In general, the largest haloes in a high-resolution run contain much resolved but bound substructure. Because we search for the $\delta = \delta_{vir}$ radius, we detect the same regions of space dozens of times for the largest haloes. To remove 'double-counted' haloes, the haloes are searched in reverse order by mass to see if they enclose the centres of any smaller haloes. If so, the smaller halo is discarded. Note that the ordering is important because three-body intersections would be non-deterministic otherwise, and throwing away haloes that only intersect is too stringent.

One limitation of this algorithm is that it presumes all haloes are spherically symmetric, which is demonstrably untrue. However, the effect on the mass function is *random*, rather than systematic, and finding the haloes with an algorithm generalized to *ellipsoidal* distributions does not change the mass function significantly, even though it changes the parameters of individual haloes. Because the haloes have finite size, one cannot perform mass-weighted correlation function analyses, for distances less than the largest halo radius (about $2–3\,h^{-1}$ Mpc in radius, typically).

The other limitation is the use of the density grid to identify halo candidates. If one considers a worst-case identification in which a large number of particles all collect in one corner of a grid cell, in order to guarantee that all nearby haloes are identified, one must draw a sphere which encloses the *entire* cell, of radius

$$r_{min} = \sqrt{3}L/N_g^{1/3}, \tag{7}$$

where L is the length of one side of the computational volume and N_g is the number of grid cells. If haloes happen to be bigger than that, then the last step of the halo catalogue generator makes it unimportant that we couldn't see nearby structure. Fortunately, halo extent is trivially related to halo mass because we have defined both where the mean overdensity is $\delta = \delta_{vir}$.

3.2 The effect of mass resolution

To what extent should you, the reader, trust the mass functions presented in this paper? To answer that, one must consider several effects. A typical feature in a mass function is that the large-mass end becomes 'wiggly', usually blamed on the scarcity of high-mass haloes combined with cosmic variance. There is a related effect at somewhat smaller masses, since very large haloes tend to have somewhat massive companions. For example, in most models in our high-resolution suite, $5\times10^{13}\,h^{-1}\,M_\odot$ objects are fairly rare, but it is common to see them as companions for $10^{15}\,h^{-1}\,M_\odot$ objects. So, the wiggles may propagate down the mass function, and cosmic variance may have a significant effect on more than just the highest mass scales.

Cosmic variance fortunately leaves a signature, in that the mass function is not smooth at high masses. However, it is quite important to figure out the limiting factors at low mass, where typical mass functions are quite smooth. What limits accuracy here are the effects of finite sized grids and finite numbers of particles.

The effect of the finite sized grid in identifying maxima in the final particle distribution was discussed above, and one must merely translate the minimum radius of a halo r_{min} to a minimum mass. Since the halo radius and mass are defined as enclosing a mean overdensity of δ_{vir}, the mass M_{vir} of a halo of radius r_{vir} is

$$M_{vir} = (1+\delta_{vir})\frac{4\pi}{3}\Omega_0\rho_c r_{vir}^3. \tag{8}$$

So, a *very* conservative mass cut is

$$M_{min} = (1+\delta_{vir})\frac{4\pi}{3}\Omega_0\rho_c\frac{(L\sqrt{3})^3}{N_g}. \tag{9}$$

Plugging in values for the high-resolution suite, the mass cut is $3.4\times10^{11}\Omega_0\,h^{-1}\,M_\odot$. For simplicity, we make the same mass cut on all models, corresponding to $\Omega_0 = 1$.

One might worry that the central density cut described in the previous section could cut too many small haloes, because the fairly long time-steps we use cause the density within the 'half-mass' radius to go down by about a factor of two if the time-step equals the stability limit (Quinn et al. 1997). We perform the central overdensity cut at $r = L/2N_g$, but the proximity restriction used in deriving equation (9) requires that halo radii in the final catalogues be at least $\sqrt{3}L/N_g$. If halo profiles fall at least as fast as r^{-1} (whereas the Navarro, Frenk & White 1997 profile says it should be much steeper than that near the virial radius), then the density fed into the central overdensity cut should be at least a factor of $2\sqrt{3} \approx 3.4$ greater than the virial density. This more than offsets the density smoothing due to time-stepping at the stability limit, so we neglect the effect of time-steps in our mass resolution analysis. Note that our time-steps are only near the stability limit for virial radii near the detection limit – otherwise, a particle takes many time-steps to cross a halo. Therefore, lowered densities due to long time-steps are only a concern for the smallest detectable haloes.

One might also worry that the quality of the force law at scales approaching the grid scale would also result in reduced central density. At the 1.7 grid cells proximity cut-off, the point–mass potential in our simulations is about 90 per cent of the correct GM/r value. With such a force law, the virial theorem requires that the density also be 10 per cent low, to maintain the same velocity dispersion. Thus, some of the smallest haloes around the mass cut will not make it into the catalogue. In practice, the density profiles for the smallest haloes are considerably noisier than 10 per cent as a result of asphericity and background particles, so we neglect the effect of an oversoftened force law.

Particle discreteness may also affect the halo mass function,

[6] Note that our definition of δ_{vir} is related to Eke et al. (1996) by $1+\delta_{vir} = \Delta_{ECF}/\Omega$. Our choice is appropriate for the density field calculations in an N-body code.

because random fluctuations may affect the detection of some of the smallest haloes. We consider here how much significance we need to make the expected number of haloes missed fewer than the number of haloes in the simulation. Because halo boundaries are defined where the mean overdensity δ is $\delta_{\rm vir}$ and the mass of a particle is

$$M_{\rm p} = \Omega_0 \rho_{\rm c} \frac{L^3}{N_{\rm p}}, \tag{10}$$

where $N_{\rm p}$ is the number of cold particles in the simulation,[7] the number of particles inside a halo of mass $M_{\rm vir}$ in a simulation box of size L is

$$N_{\rm vir} = \frac{M_{\rm vir} N_{\rm p}}{\Omega_0 \rho_{\rm c} L^3}. \tag{11}$$

For counting N particles within r, the random variation in number is $\sigma = \sqrt{N}$. Let us suppose there are $N_{\rm h}$ haloes above a given mass, and we wish to detect them all. We presume that counting haloes is a Gaussian process and state that the n-sigma uncertainty in the detection of the haloes corresponds to incorrectly detecting or missing a fraction $\mathrm{erfc}(n/\sqrt{2})$ of the haloes. We require detection of all haloes, so the fraction missed should be less than $1/\rho_{\rm h} L^3$, where ρ is the number density of haloes above the mass cut-off, and L^3 is the volume of the simulation box where haloes are identified. Inverting, we need detections of $\sqrt{2}\,\mathrm{erfc}^{-1}(1/\rho_{\rm h} L^3)$ sigma. The density $\rho_{\rm h}$ should really come from the Press–Schechter approximation, given a desired mass cut-off, but the inverse complementary error function is extremely insensitive to the value of its argument, once it becomes much less than one. As an example, for $\rho_{\rm h} = 1\,h^3\,\mathrm{Mpc}^{-3}$ (appropriate for a mass cut-off a little below $10^{11}\,h^{-1}\,\mathrm{M}_\odot$ for most models), we need to have at least 4.7σ detections of all haloes. Less significant detections mean it is likely some of them have been missed by random fluctuations. This means every halo must contain at least 23 particles. More generally,

$$N_{\rm min} = 2\left[\mathrm{erfc}^{-1}\left(\frac{1}{\rho_{\rm h} L^3}\right)\right]^2 \tag{12}$$

for the rather liberal restriction that we only require detection of the halo.

As an alternative cut-off criterion, requiring a 10 per cent or less 1σ error in mass is a more stringent requirement, and every halo must have at least 100 particles, since mass is determined by counting particles within several radii. If one requires a fractional error of f for a minimum halo mass of $M_{\rm min}$, one needs at least

$$N_{\rm p} = \frac{\Omega_0 \rho_{\rm c} L^3}{f^2 M_{\rm min}} \tag{13}$$

particles in the simulation. The parameters used, and the effective f they allow, are shown in Table 2. Fig. 5 shows that, with grid sizes and mean interparticle spacings of the order of those used in our suite, the effect of lowering either the grid size or the mean interparticle spacing by a factor of two does not significantly affect the mass function. For this test, we raised the threshold for halo candidate identification from $\delta = 50$ in one cell to $\delta = 70$ because one isolated cold particle in the high $N_{\rm g}$ case gives $1 + \delta = 51.2$.

[7]For simplicity, we consider the significance of models with only one particle mass. For CHDM-2ν, a given mass will always be represented by more particles than in SCDM. So, one can get a conservative estimate of the significance by only considering the cold particles.

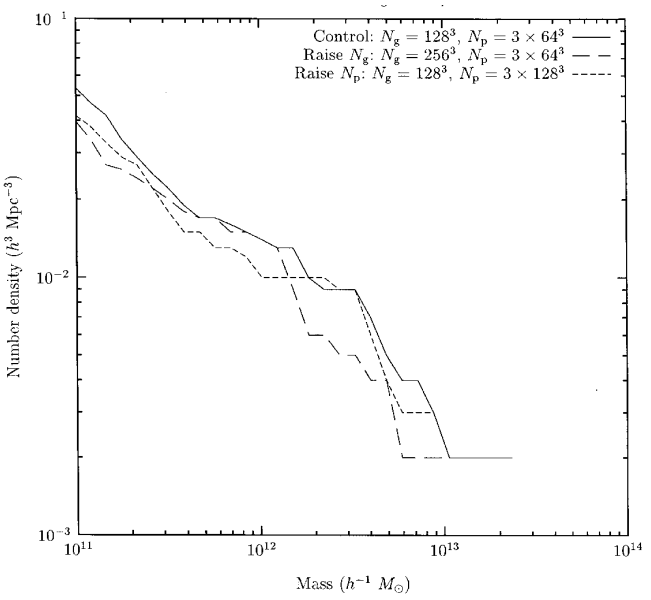

Figure 5. Effect of raising the number of particles or the number of grid cells by a factor of 8 in a very small CHDM-2ν $10\,h^{-1}$ Mpc simulation with $N_{\rm g} = 128^3$ and $N_{\rm p} = 3 \times 64^3$. The mass functions are not significantly different. A somewhat low mass cut-off of $10^{11}\,h^{-1}\,\mathrm{M}_\odot$ has been applied. The high-resolution suite has a linear cell size that is slightly smaller than the $N_{\rm g} = 128^3$ runs shown in this figure.

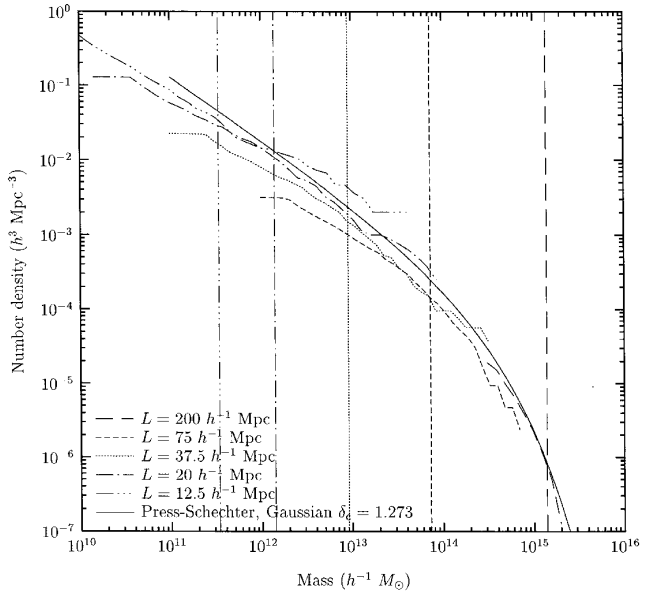

Figure 6. Effect of grid size on mass functions. The curves represent very small simulations of various sizes. The Press–Schechter model was tuned to match the cluster-scale part of the mass function in the largest box. Note that the envelope mirrors the Press–Schechter curve reasonably well, but each individual mass function has a power-law index that is too shallow. Mass functions are limited at the large-mass end by statistics – one simply runs out of enough space to create objects in – and on the small-mass end by some fraction of the haloes becoming as small as two grid cells, which means it is not guaranteed that the halo can be resolved from its neighbours, particularly if they are also small haloes. The vertical lines represent the lower limit in mass for each run, above which all haloes can be detected.

To explicitly test the effect of grid sizes on our mass functions, we ran five small simulations of the CHDM-2ν model with $N_g = 192^3$ grid cells and $N_p = 3 \times 64^3$ particles, with various-sized boxes. Though these simulations are too small to generate meaningful mass functions on their own, collectively their upper envelope does match the Press–Schechter formula reasonably well, for $\delta_{c,g} = 1.2$ with a Gaussian filter. Fig. 6 shows the five different mass functions. Also shown are lower mass cuts, determined for every model using equation (9). Above the mass cut-offs, every mass function agrees with the one for the next smaller box. Well below the mass cut-offs, the mass function slopes are not steep enough, but they agree with the neighbouring curves for significant distances below the mass cuts, so it may be reasonable to extrapolate the mass function further. Every halo detected by the halo finder is represented in the figure, and the locations of the lower mass cuts are indicated by vertical lines. This test could conceivably overproduce clusters because of the extremely poor force and mass resolutions in the largest volume run – a cell width is about the size of an Abell radius. This δ_c result does persist for much larger simulations, as discussed below.

4 RESULTS

The connection between simulations and observations is still fairly uncertain, and the least well-determined portion of it is the galaxy identification procedure. It is therefore helpful to do as much analysis as one can using quantities that are insensitive to the details of galaxy formation. Currently, only bulk flow motions (Kolatt & Dekel 1997) provide a meaningful *matter* power spectrum, but the large smoothing required means that the comparison is best made to the linear power spectrum (see Fig. 3). When investigating quantities derived from observations of galaxies (as the vast majority of astronomical observations are), one is forced to make assumptions based on expections about the nature of galaxy bias, for example the usual expectation that galaxies are more clustered than the dark matter. Fig. 7 shows non-linear real-space dark matter power spectra for all our models, compared to the APM real-space galaxy power spectrum (Baugh & Efstathiou 1994). The OCDM model requires significant antibiasing and the ΛCDM model requires even more. There is no evidence for such strong antibiasing, and it is very difficult to explain physically, especially on such large scales (cf. Yepes et al. 1997; Kauffmann, Nusser & Steinmetz 1997). Additional arguments against strongly scale-dependent antibiasing are given in Klypin et al. (1996, hereafter KPH96).

The process of galaxy formation is not well understood, so one could argue that perhaps there *is* some mechanism that would give us strong antibiasing. We have created an extreme model for galaxy formation designed to produce as much antibias as possible (cf. KPH96). Everywhere in the density grid, if there is more than $2.1 \times 10^9\, h^{-1}\, M_\odot$ in a grid cell, we presume one galaxy forms there. That mass corresponds to slightly more than the mass due to one isolated particle in the high-resolution SCDM and TCDM simulations (which have the most massive particles in the suite). Such a limit is necessary to prevent placing excess power in the voids due to vestiges of the initial grid there. This is a highly unreasonable model for galaxy formation, as it says that the density of $\gtrsim 2 \times 10^{11}\, h^{-1}\, M_\odot$ galaxies in the core of the Coma cluster should be the same as in the local group, and this is clearly ruled out observationally. However, even though there is significant antibias on small scales, it is only visible at scales smaller than about $k = 1\, h\,\mathrm{Mpc}^{-1}$ (see Fig. 8), whereas antibiasing is needed on scales

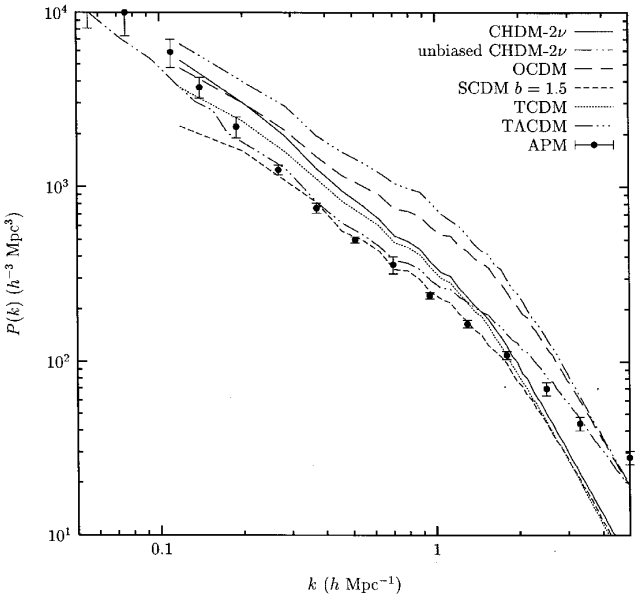

Figure 7. Non-linear real-space dark matter power spectra, compared to the APM real-space galaxy power spectrum (Baugh & Efstathiou 1994) of galaxy number-count fluctuations. The simulation power spectra shown here are a composite of the high- and low-resolution suites, where data from a model's high-resolution run are used at large k and low-resolution data are used at small k. Two different high-resolution runs of the SCDM case are shown as a guide to how large cosmic variance is. The power in the second SCDM realization is 20–30 per cent lower than that in the first realization for $0.3 \lesssim k \lesssim 1\, h\,\mathrm{Mpc}^{-1}$. The APM data are presumably biased with respect to the matter power spectrum, and yet the OCDM, TCDM, and TΛCDM cases require the APM data to be significantly *antibiased* with respect to the dark matter, with $b^2 \sim 0.6$ for OCDM and TCDM and $b^2 \sim 0.5$ for TΛCDM at $k \sim 1\, h\,\mathrm{Mpc}^{-1}$. If APM misses galaxies in clustered regions, that would give a low-power spectrum on scales of $k \gtrsim 1\, h\,\mathrm{Mpc}^{-1}$ (see text).

larger than that in order for OCDM or TΛCDM to be consistent with the APM power spectrum. Note that a possible way out of the antibiasing requirement is to note that the APM survey is incomplete in clustered regions, which will raise the 'true' power spectrum above the APM measurement on small scales (Zabludoff, private communication).

The APM power spectrum is not the only power spectrum that has been measured. However, to compare to other measurements, it is usually required to calculate model redshift space power spectra. Going to redshift space significantly reduces power on scales of interest, since typical dispersion velocities of 1000–2000 km s^{-1} in clusters correspond to a scatter of 10–$20\, h^{-1}$ Mpc in distance. In performing this operation on particles, the power should be viewed as a lower bound, because there may be significant velocity bias (Carlberg, Couchman & Thomas 1990; Summers, Davis & Evrard 1995), meaning the power perhaps should not be supressed *quite* as much, and galaxy formation will further raise the power. Fig. 9 shows the models' redshift space power spectra, compared to the combined CfA2 and SSRS2 redshift space power spectrum (da Costa et al. 1994). Given our choices of model normalization and cosmological parameters, the TΛCDM matter power spectrum is nicely consistent with the observed galaxy power spectrum, but that leaves *no* room for galaxy formation or velocity bias effects. As for the real-space non-linear power spectrum comparison (Fig. 7), this requires significant antibiasing for TΛCDM on scales of 0.3–$1\, h\,\mathrm{Mpc}^{-1}$. Note that undersampling the velocity field will miss the

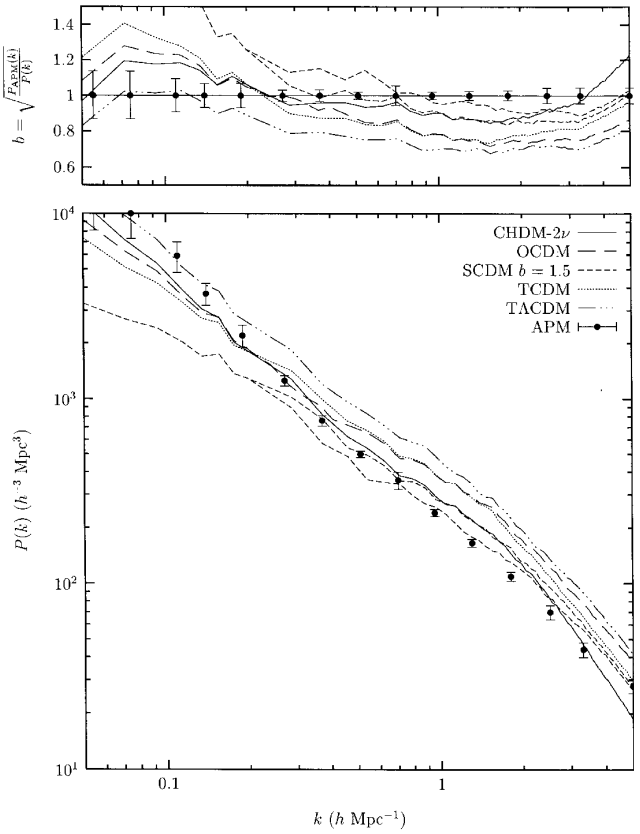

Figure 8. Non-linear power spectra, presuming an extreme scale-dependent biasing scheme. The density field has been set to 'on' at any cell containing mass exceeding the largest particle mass in the $75\,h^{-1}$ Mpc suite, $2.1 \times 10^9\,h^{-1}\,\mathrm{M}_\odot$, and 'off' everywhere else. That mass cut is most likely lower than anything that could make it into the CfA2 or APM catalogues, except if one assumes an impossibly small mass-to-light ratio. The result of such a bizarre galaxy identification scheme is a bias on large scales, due to clearing out the void regions, and an antibias on small scales, due to removing the high peaks in density. We do comparisons with the high-resolution suite because the low-resolution suite particle mass is too high.

large velocities by making the haloes physically larger, so it does not make sense to perform redshift space comparisons on the large volume suite.

The simplest halo-related quantity to investigate is the number density of bound objects as a function of mass. Such 'mass functions' and close relatives such as the X-ray temperature function (as in Eke et al. 1996, for example) are often estimated from the Press–Schechter approximation instead of from simulations. Though it has been checked against scale-free simulations (Efstathiou et al. 1988; Bond et al. 1991; Lacey & Cole 1994) and against specific SCDM, ΛCDM and CHDM models (Carlberg & Couchman 1989; Jain & Bertschinger 1994; Klypin et al. 1995; Walter & Klypin 1996; Bond & Myers 1996), previous studies have focused only on a narrow range of masses, typically at the cluster scale. With our large simulations, we can check the approximation over four orders of magnitude in mass. The Press–Schechter formula we use is Klypin et al. (1995), equations (1–2), evaluated at $z = 0$:

$$N(>M) = \sqrt{\frac{2}{\pi}}\frac{\delta_\mathrm{c}}{\alpha_\mathrm{m}}\int_r^\infty \frac{\epsilon(r')}{\sigma^3(r')}\exp\left[\frac{-\delta_\mathrm{c}^2}{2\sigma^2(r')}\right]\frac{\mathrm{d}r'}{r'^3}, \tag{14}$$

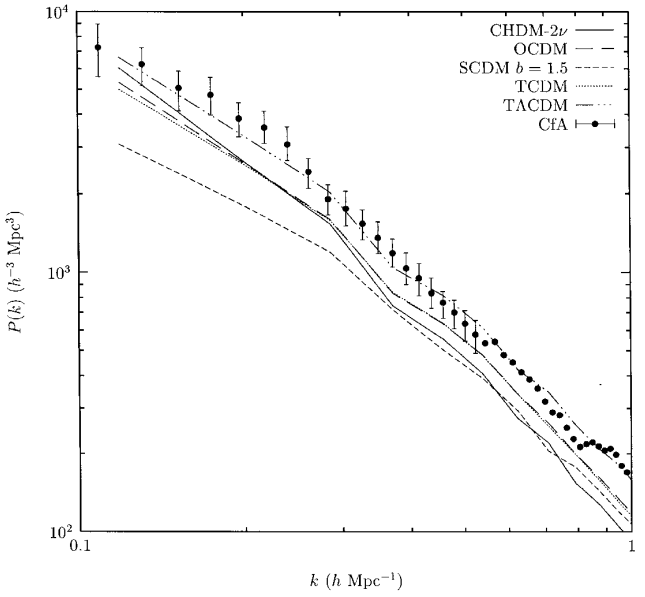

Figure 9. Redshift-space power spectrum, compared to the combined CfA2 and SSRS2 redshift-space power spectrum (da Costa et al. 1994). Notice that, while ΛCDM is a good match to this power spectrum, there is no room for galaxy formation or velocity bias.

where

$$\epsilon(r) = \frac{1}{2\pi}\int_0^\infty k^3 P(k) W(kr)\frac{\mathrm{d}W(kr)}{\mathrm{d}(kr)}\mathrm{d}k, \tag{15}$$

$$\sigma^2(r) = \frac{1}{2\pi^2}\int_0^\infty k^2 P(k) W^2(kr)\mathrm{d}k, \tag{16}$$

$$W(x) = \begin{cases} \dfrac{3}{x^3}[\sin(x) - x\cos(x)] & \text{top hat} \\ \mathrm{e}^{-\mathrm{x}^2/2} & \text{Gaussian} \end{cases}, \tag{17}$$

$$r = \left(\frac{M}{\alpha_\mathrm{m}\rho_\mathrm{c}\Omega_0}\right)^{\frac{1}{3}} \tag{18}$$

and α_m is $4\pi/3$ for a top hat window function, and $(2\pi)^{3/2}$ for a Gaussian window function.

Fig. 10 shows the cumulative mass functions estimated from both suites of simulations, and Table 3 shows the Press–Schechter parameters used in that figure. Note that in the overlapping region, the two sets of simulation mass functions are consistent, and that *the high resolution results are a significant factor of 1.5–2 below the Press–Schechter estimates for all models at the intermediate mass of* $10^{13}\,h^{-1}\,\mathrm{M}_\odot$ *and below.*

This result has been verified recently by other groups. Bryan & Norman (1998) see a somewhat stronger discrepancy at $10^{14}h^{-1}\,\mathrm{M}_\odot$, using a spherical overdensity method, for cosmological parameters very close to our CHDM-2ν, OCDM and SCDM choices (though with substantially larger grid cell sizes for OCDM and SCDM). Somerville et al. (in preparation) also see an equivalent discrepancy in the differential multiplicity function $n(M)$ at $z = 0$ in the τCDM cosmology, for which the power spectrum is very similar to our CHDM-2ν. This result depends upon a completely independent simulation (Jenkins et al. 1998) modelled using adaptive $\mathrm{P}^3\mathrm{M}$, with haloes identified using the 'friends-of-friends' method. The halo mass function for the SCDM model from the Jenkins et al. (1998) simulations is virtually identical to ours (G. Lemson, private communication). Given these confirmations, we do not believe

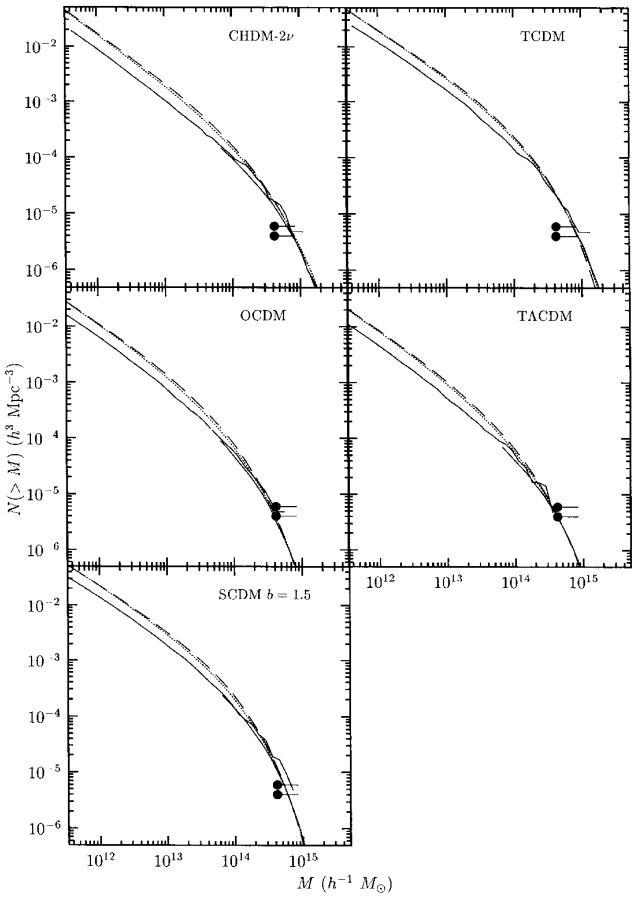

Figure 10. Cumulative halo mass functions, with Press–Schechter fits. In each panel, the relevant mass functions estimated from the two simulation suites are shown by the full curves. Small mass cuts have been applied at $M = 3.4 \times 10^{11}\, h^{-1}\,\mathrm{M}_\odot$ and $2.2 \times 10^{13}\, h^{-1}\,\mathrm{M}_\odot$, for the large and small volume simulations, respectively. Each panel also shows Gaussian (dashed curves) and top hat (dotted curves) Press–Schechter mass functions, with $\delta_{\mathrm{c,t}}$ and $\delta_{\mathrm{c,g}}$ adjusted to agree with the large-volume simulations at $5.5 \times 10^{14}\, h^{-1}\,\mathrm{M}_\odot$. The values of $\delta_{\mathrm{c,t}}$ and $\delta_{\mathrm{c,g}}$ used are given in Table 3. The data points correspond to the observations of BGGMM93 and WEF93, as in Fig. 1.

Table 3. Press–Schechter fits to simulation mass functions.

Model	$\delta_{\mathrm{c,t}}$	$\delta_{\mathrm{c,g}}$
CHDM-2ν	1.571	1.273
OCDM	1.693	1.293
SCDM $b = 1.5$	1.672	1.236
TCDM	1.630	1.252
TΛCDM	1.732	1.355

$\delta_{\mathrm{c,t}}$ and $\delta_{\mathrm{c,g}}$ have been chosen to get the same number density of clusters with $M > 5.5 \times 10^{14}\, h^{-1}\,\mathrm{M}_\odot$ as the large-volume simulation, for each model.

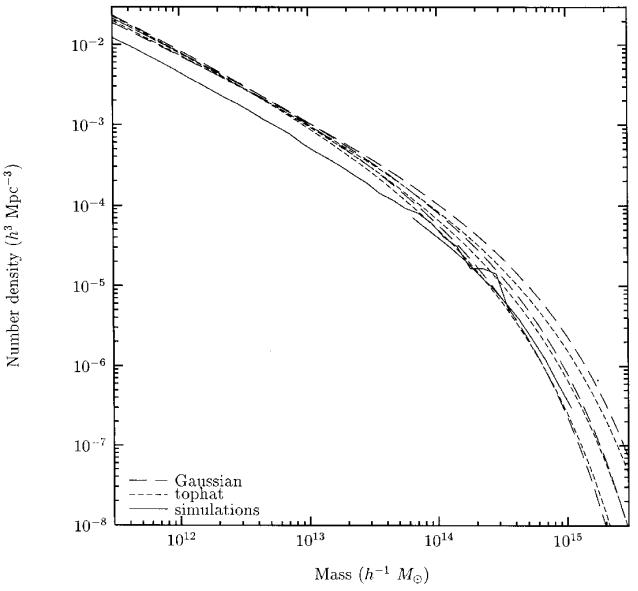

Figure 11. Press–Schechter mass functions for TΛCDM. The high- and low-density TΛCDM mass functions from simulations are shown in the solid curves. From top to bottom at $M = 10^{15}\, h^{-1}\,\mathrm{M}_\odot$, the long-dashed curves show Press–Schechter mass functions with Gaussian filters for $\delta_{\mathrm{c,g}} = 1.0$, 1.2, and 1.4, and the short-dashed curves show top hat filters for $\delta_{\mathrm{c,t}} = 1.4$, 1.6, and 1.8. Press–Schechter mass functions can be made to agree with our simulations for masses above about $5 \times 10^{13}\, h^{-1}\,\mathrm{M}_\odot$, but not for masses smaller than that.

that the medium-mass discrepancy we see is an artefact of our simulation method or halo finding algorithm.

As Fig. 11 shows, the intermediate and low-mass discrepancy *cannot* be fixed by adjusting the value of δ_{c}, particularly at a mass of $\sim 5 \times 10^{12}\, h^{-1}\,\mathrm{M}_\odot$, where the curves cross. Our values of $\delta_{\mathrm{c,t}}$ and $\delta_{\mathrm{c,g}}$ are consistent with Borgani et al. (1997b), except we find that the CHDM-2ν δ_{c} values are not significantly different from the other models. The $\delta_{\mathrm{c,t}}$ values we find for the top hat case are consistent with the spherical collapse model.

The simulation mass functions in Fig. 10 fall below the Press–Schechter predictions for most of their range. For example, in the SCDM high-resolution run, only 60 per cent of the particles are within haloes with $M > 3.4 \times 10^{11}\, h^{-1}\,\mathrm{M}_\odot$ at $z = 0$. The Press–Schechter prediction is only very slightly larger, about 62 per cent for $\delta_{\mathrm{c,t}} = 1.672$ and 65 per cent for the spherical collapse value $\delta_{\mathrm{c,t}} = 1.686$. The mass deficit arising from the smaller abundance of low-mass haloes in the simulations is almost completely compensated for by a small excess of very large clusters. The Press–Schechter approximation assumes that all the mass must be in haloes of *some* size, and this analysis indicates that a significant fraction of the mass of the universe should be in small haloes. The Press–Schechter approximation indicates that for SCDM, as much as 20 per cent of the mass is in haloes as small as $10^9\, h^{-1}\,\mathrm{M}_\odot$, which is not identifiable in any present-day cosmological simulation. The simulations show a significant amount of matter that is not in collapsed objects. Most of the mass lies in filaments connecting the clusters, many of which have only a few identified haloes on them. It is conceivable that much of this mass may be unresolved haloes, since any N-body simulation must have a resolution and/or time-step limit below which forces are 'soft,' resulting in disruption of structure

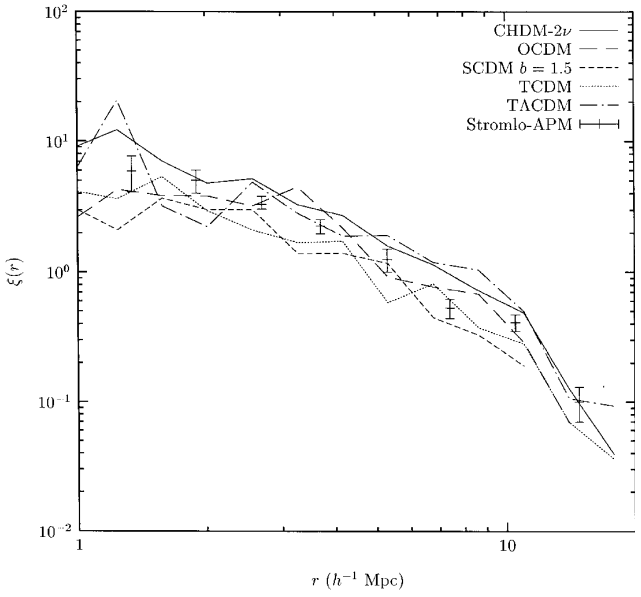

Figure 12. Halo mass-weighted correlation function. Only haloes with mass above $3\times10^{11}\,h^{-1}\,\mathrm{M}_\odot$ are included, and all pairs are weighted by the product of the two masses. Such a weighting is a simple countermeasure for the overmerging problem. The error bars are the Stromlo–APM autocorrelation function (Loveday et al. 1995).

smaller than the limit. Such a mechanism must be present, since filament haloes are necessarily not very big, but it is not clear how much of the mass that can account for.

Our two low-Ω_0 models produce fewer clusters in simulations than the other models (Fig. 10). If X-ray temperature cluster masses are correct, this presents no problem for those models. However, if the indications of larger cluster masses from gravitational lensing are correct, the low-Ω_0 models require revision by using less tilt (in the case of TΛCDM) or a larger value of H_0. The former would help lessen the disagreement with high-multipole cosmic microwave background measurements (Fig. 2), as a weaker tilt would raise the first Doppler peak, but will lead to the need for even stronger antibias to reconcile small-scale power with the APM observations. If X-ray temperature masses are correct, our parameters for TCDM and CHDM-2ν produce too many clusters. For CHDM-2ν, the normalization used here was actually about 10 per cent higher than the preferred four-year *COBE* normalization, so reducing the normalization by this factor would probably be enough, though this will exacerbate early structure formation problems. For TCDM, the only options are either to increase the tilt, which is highly disfavoured by the small-angle cosmic microwave background data as already noted, or to further reduce the Hubble parameter, which is also strongly disfavoured by observations.

The statements above all take the *COBE* normalization as a fixed constraint. Alternatively, we could turn the problem around and use the clusters to determine normalizations and tilts, with H_0 (and Ω_0 and Ω_Λ) as given. This is explored further in Gross et al. (in preparation).

We would now like to investigate statistics such as correlation functions, void probability functions (Ghigna et al. 1997), shape statistics (Davé et al. 1997), and other sophisticated statistics. However, to compare these to observations, we need to know how many galaxies form in each halo. Previous studies (KNP97; Nolthenius, Klypin & Primack 1997; Ghigna et al. 1997, for example) have used ad hoc 'break-up' prescriptions to assign galaxies to haloes. We intend to populate our haloes with galaxies using a more physically motivated approach (as in Kauffmann et al. 1997) based on semi-analytic models including simplified treatments of gas processes, star formation, supernova feedback, and galaxy–galaxy merging (Somerville 1997; Somerville & Primack 1998). As a result, we do not attempt to include any complicated galaxy identification algorithms here.

For certain statistics, one can partially compensate for the effect of overmerging by *mass weighting*. This approach is less than ideal because it does not restore the small-scale *spatial* information lost in the overmerging process. Mass weighting is equivalent to presuming a halo contains a number of galaxies proportional to its mass, and putting all the galaxies at the centre of the halo. In effect, this clears out regions of space around the centres of the largest haloes, equal to their radii, and therefore loses information on scales smaller than the largest halo radius (typically 2–$3\,h^{-1}$ Mpc). Since very massive haloes are rare objects for physically interesting cosmological models, all mass weighted statistics must be unduly influenced by small-number statistical noise.

We calculate the mass-weighted autocorrelation function for the high-resolution runs, and the results are shown in Fig. 12. In this figure, a halo mass cut of $M = 3\times10^{11}\,h^{-1}\,\mathrm{M}_\odot$ was used, although the mass weighting makes it insensitive to the mass cut. The mass weighting creates a spread in the correlation values large enough to prevent the test from discriminating among models. To within the spread visible in Fig. 12, all models are roughly consistent with the Stromlo–APM autocorrelation function (Loveday et al. 1995). However, there are a few trends visible in the figure. SCDM and TCDM are systematically lower in amplitude than the other models, but the effect is not very significant given the spread.

5 CONCLUSIONS

We have run two suites of simulations with 57 million cold particles in boxes of 75 and $300\,h^{-1}$ Mpc, with the goal of studying interesting variants of the CDM family of cosmological models. In this paper, we have made preliminary comparisons of the $z = 0$ simulation outputs to data for all models. In Smith et al. (1998), we used the lower-resolution suite, plus some additional simulations, to generalize the Peacock & Dodds (1994, 1996) procedure for recovery of the linear power spectrum corresponding to a given cosmological model from observational data. In Wechsler et al. (1998), we showed that the most massive haloes at redshifts $z \sim 3$, or objects that trace their distribution, can account for the observed clustering of Lyman-break objects (Steidel et al. 1998) for all cosmologies except SCDM. More detailed comparisons with observations require assumptions about galaxy formation and will be treated in subsequent work. Subject to the usual caveats about the uncertainty of galaxy formation, we reach the following conclusions in the present paper.

(i) Based on the results of KPH96, who found that ΛCDM models with $\Omega_0 \sim 0.3$ would require strong scale-dependent antibias in order to be consistent with the APM power spectrum (Baugh & Efstathiou 1994), we investigated a variant of the ΛCDM model with $\Omega_0 = 0.4$ and a tilt of $n = 0.9$. We find that this model still requires a large antibias of $b^2 \equiv P_{\mathrm{APMgal}}/P_{\mathrm{dm}} \sim 0.5$ at $k = 1\,h\,\mathrm{Mpc}^{-1}$. Even in a simple model in which galaxies are extremely antibiased with respect to dark matter haloes, the problem persists on scales of

$r \sim 6h^{-1}$ Mpc, because this scale is larger than the size of individual haloes. To get antibias on these scales, there would have to be many 'barren' haloes containing *no* galaxies. OCDM and TCDM are only slightly better, still requiring a strong antibias of $b^2 \sim 0.6$. Other models considered require a weaker antibias at that scale.

(ii) The TΛCDM dark matter redshift-space power spectrum agrees very well with the redshift-space galaxy power spectrum from CfA2+SSRS2 (da Costa et al. 1994). This leaves no room for the 'positive' bias expected in normal galaxy formation, or for velocity biases. For comparison, OCDM and TCDM each have room for a modest bias of $b^2 \sim 1.2$ at $k = 0.5\,h\,\mathrm{Mpc}^{-1}$, and CHDM-2$\nu$ and SCDM each need $b^2 \sim 1.5$.

(iii) All models considered here are consistent with the Stromlo–APM real-space correlation function (Loveday et al. 1995) on scales of 2–$20\,h^{-1}$ Mpc, largely as a result of a large spread in the model estimates of the correlation function because of mass weighting and small-number statistics for large-mass objects.

(iv) The Press–Schechter approximation fits the abundance of cluster-mass haloes very well, with top hat $\delta_{c,t} = 1.57-1.73$ and Gaussian $\delta_{c,g} = 1.27-1.35$. However, it overpredicts the number density of galaxy and small group mass objects by a factor of $\sim$2, only weakly dependent on cosmology, and very weakly dependent on δ_c. On mass scales of $\sim 5 \times 10^{12}\,h^{-1}\,\mathrm{M}_\odot$, it is not possible to compensate for the discrepancy by adjusting δ_c within reasonable bounds.

In summary, we conclude that none of the models we have investigated can be strongly ruled out by the kind of analysis performed here. The CHDM-2ν model gives the best overall agreement with the linear and non-linear tests we have considered here, assuming that galaxies are positively biased with respect to the dark matter. Gawiser & Silk (1998) have shown that a similar CHDM model with $\Omega_\nu = 0.2$ in $N_\nu = 1$ neutrino species is a much better fit to microwave background and galaxy distribution data than any other popular cosmological model. Preliminary analysis based on the dark matter alone has shown that the related CHDM-2ν model considered in this paper is plausibly consistent with high-redshift observations of Lyman-break galaxies (Wechsler et al. 1998) and damped Lyman-α systems (Klypin et al. 1995), but it remains to be seen whether this model will produce enough early galaxy formation once a more realistic treatment of gas processes and star formation is included. More detailed modelling of galaxy formation will also be necessary to determine whether the small-scale clustering properties of the low-Ω_0 models are indeed inconsistent with the observations. In any case we conclude that models with $\Omega_0 \sim 0.5$ are in better overall agreement with the observations than the lower values ($\Omega_0 \sim 0.2$–0.3) usually considered (e.g. Jenkins et al. 1998). A powerful constraint on Ω_0, the evolution of cluster abundance with redshift, will be considered in a companion paper (Gross et al., in preparation).

6 ACKNOWLEDGMENTS

MAKG and JRP were supported by NSF and NASA grants at the University of California at Santa Cruz, RSS was supported by a GAANN fellowship, and JH and AK were supported by NSF and NASA grants at New Mexico State University. The simulations were run on the IBM SP2 at the Cornell Theory Center, Cornell University, Ithaca, NY, USA, and computer time for analysis was provided by Sandra Faber and the DEIMOS project at the University of California at Santa Cruz.

REFERENCES

Bardeen J. M., Bond J. R., Kaiser N., Szalay A. S., 1986, ApJ, 304, 15 (BBKS)
Bartlett J. G., Blanchard A., Silk J., Turner M. S., 1995, Sci, 267, 980
Baugh C. M., Efstathiou G., 1994, MNRAS, 267, 323
Bernardeau F., Juszkiewicz R., Dekel A., Bouchet F., 1995, MNRAS, 274, 20
Biviano A., Girardi M., Giuricin G., Mardirossian F., Mezzetti M., 1993, ApJ, 411, L13 (BGGMM93)
Blumenthal G. R., Faber S. M., Primack J. R., Rees M. J., 1984, Nat, 311, 517
Bond J. R., Myers S. T., 1996, ApJS, 103, 41
Bond J. R., Cole S., Efstathiou G., Kaiser N., 1991, ApJ, 379, 440
Borgani S., Gardini A., Girardi M., Gottlöber S., 1997a, New Astron., 2, 119
Borgani S. et al., 1997b, New Astron., 1, 321
Bryan G. L., Norman M.L., 1998, ApJ, 495, 80
Bunn E. F., White M., 1997, ApJ, 480, 6
Burles S., Tytler D., 1997, ApJ, 499, 699
Burles S., Tytler D., 1998, ApJ, 499, 699
Carlberg R. G., Couchman H. M. P., 1989, ApJ, 340, 47
Carlberg R. G., Couchman H. M. P., Thomas P. A., 1990, ApJ, 352, L29
Chaboyer B., Demarque P., Kernan P. J., Krauss L. M., 1998, ApJ, 494, 96
Couchman H. M. P., 1991, ApJ, 368, L23
da Costa L. N., Vogeley M. S., Geller M. J., Huchra J. P., Park C., 1994, ApJ, 437, L1
Davé R., Hellinger D., Primack J. R., Nolthenius R., Klypin A., 1997, MNRAS, 284, 607
Davis M., Efstathiou G., Frenk C. S., White S. D. M., 1985, ApJ, 292, 371
Dekel A., Rees M. J., 1994, ApJ, 422, L1
Efstathiou G., Frenk C. S., White S. D. M., Davis M., 1988, MNRAS, 235, 715
Eke V. R., Cole S., Frenk C. S., 1996, MNRAS, 282, 263
Gawiser E., Silk J., 1998, Sci., 280, 1405
Gelb J. M., Bertschinger E., 1994, ApJ, 436, 467
Ghigna S. Borgani S., Tucci M., Bonometto S. A., Klypin A., Primack J. R., 1997, ApJ, 479, 580
Górski K. M., Banday A. J., Bennett C. L., Hinshaw G., Kogut A., Smoot G. F., Wright E. L., 1996, ApJ, 464, L11
Gratton R. G., Fusi Pecci F., Carretta E., Clementini G., Corsi C. E., Lattantzi M., 1998, ApJ, 491, 749
Gross M. A. K., 1997, PhD thesis, Univ. California, Santa Cruz (http://fozzie.gsfc.nasa.gov/#dissertation)
Henry J. P., Arnaud K. A., 1991, ApJ, 372, 410
Hockney R. W., Eastwood J. W., 1988, Computer Simulation Using Particles. Institute of Physics Publishing, Philadelphia PA
Holtzman J. A., 1989, ApJS, 71, 1
Hu W., Sugiyama N., 1996, ApJ, 471, 542
Hu W., White M., 1997, ApJ, 486, L1
Jain B., Bertschinger E., 1994, ApJ, 431, 495
Jenkins A. et al., 1998, ApJ, 499, 20
Kates R. E., Kotok E. V., Klypin A., 1991, A&A, 243, 295
Kauffmann G., Charlot S., 1994, ApJ, 430, L97
Kauffmann G., Nusser A., Steinmetz M., 1997, MNRAS, 286, 795
Klypin A., Holtzman J., Primack J., Regös E., 1993, ApJ, 416, 1
Klypin A., Borgani S., Holtzman J., Primack J., 1995, ApJ, 444, 1
Klypin A., Primack J., Holtzman J., 1996, ApJ, 466, 13 (KPH96)
Klypin A., Gottlöber S., Kravtsov A. V., 1997a, preprint (astro-ph/9708191)
Klypin A., Nolthenius R., Primack J., 1997b, ApJ, 474, 533 (KNP97)
Kolatt T., Dekel A., 1997, ApJ, 479, 592
Kravtsov A. V., Klypin A., Khokhlov A. M., 1997, ApJS, 111, 73
Lacey C., Cole S., 1994, MNRAS, 271, 676
Liddle A. R., Lyth D. H., Roberts D., Viana P. T. P., 1996, MNRAS, 278, 644 (LLRV96)
Lineweaver C. H., Barbosa D., 1998, ApJ, 496, 624
Loveday J., Maddox S. J., Efstathiou G., Petersen B. A., 1995, ApJ, 442, 457
Miralda-Escudé J., Babul A., 1995, ApJ, 449, 18

Monaco P., 1995, ApJ, 447, 23
Navarro J. F., Frenk C. S., White S. D. M., 1997, ApJ, 490, 493
Netterfield C. B., Devlin M. J., Jarosik N., Page L., Wollack E. J., 1997, ApJ, 474, 47
Nolthenius R., Klypin A., Primack J. R., 1997, ApJ, 480, 43
Nusser A., Dekel A., 1993, ApJ, 405,437
Peacock J. A., Dodds S. J., 1994, MNRAS, 267, 1020
Peacock J. A., Dodds S. J., 1996, MNRAS, 280, L19
Pen U. L., 1998, ApJ, 498, 60
Platt S. R., Kovac J., Dragovan M., Petersen J. B., Ruhl J. E., 1997, ApJ, 475, L1
Pogosyan D. Y., Starobinsky A. A., 1995, in Muckett J. P., Gottlöber S., Müller V., eds, International Workshop on Large Scale Structure in the Universe. World Scientific Press, River Edge, NJ
Press W. H., Schechter P., 1974, ApJ, 187, 425
Primack J. R., Holtzman J., Klypin A., Caldwell D. O., 1995, Phys. Rev. Lett., 74, 2160
Quinn T., Katz N., Stadel J., Lake G., 1997, preprint (astro-ph/9710043)
Reid I. N., 1997, AJ, 114, 161
Scott P. F. et al., 1996, ApJ, 461, L1
Seljak U., Zaldarriaga M., 1996, ApJ, 469, 437
Smith C. C., Klypin A., Gross M. A. K., Primack J. R., Holtzman J., 1998, MNRAS, in press (astro-ph/9702099)
Smoot G. F. et al., 1992, ApJ, 396, L1
Somerville R. S., 1997, PhD thesis, Univ. California, Santa Cruz (http://www.fiz.huji.ac.il/rachels/thesis.html)
Somerville R., Primack J., 1998, MNRAS, submitted, astro-ph/9802268
Squires G., Kaiser N., Babul A., Fahlman G., Woods D., Neumann D. M., Böringer H., 1996, ApJ, 461, 572
Squires G., Neumann D. M., Kaiser N., Arnaud M., Babul A., Böhringer H., Fahlman G., Woods D., 1997, ApJ, 482, 648
Steidel C. C., Adelberger K. L., Dickinson M., Giavalisco M., Pettini M., Kellogg M., 1998, ApJ, 492, 428
Summers F. J., Davis M., Evrard A. E., 1995, ApJ, 454, 1
Tegmark M., 1996, ApJ, 464, L35
Tytler D., Fan X., Burles S., 1996, Nat, 381, 207
Viana P. T. P., Liddle A. R., 1996, MNRAS, 281, 323
Walter C., Klypin A., 1996, ApJ, 462, 13
Wechsler R. H., Gross M. A. K., Primack J. R., Blumenthal G. R., Dekel A., 1998, ApJ, in press (astro-ph/9712141)
White S. D. M., Efstathiou G., Frenk C. S., 1993, MNRAS, 262, 1023 (WEF93)
Wu X. P., Fang L. Z., 1996, ApJ, 467, L45
Wu X. P., Fang L. Z., 1997, ApJ, 483, 62
Xu G., 1995, ApJS, 98, 355
Yepes G., Kates R., Khokhlov A., Klypin A., 1997, MNRAS, 284, 235
Zel'dovich Y. B., 1970, A&A, 5, 84